ORIGINAL PAPER

Electroanalysis with a single microbead of phosphate binding resin (FerrIX™) mounted in epoxy film

Abigail K. Thompson[1] · Klaus Mathwig[2] · Philip J. Fletcher[3] · Rémi Castaing[3] · Frank Marken[1]

Abstract

Commercial resin microbeads are widely applied in ion exchange and extraction. Here, a single anion-selective and phosphate binding resin microbead (FerrIX™) is mounted into an epoxy membrane and investigated by 4-electrode membrane voltammetry and membrane impedance spectroscopy. Anion transport properties are observed to dominate associated with three distinct potential domains: (I) a low bias ohmic potential domain (dominant at high electrolyte concentration), (II) a concentration polarisation potential domain, and (III) an over-limiting potential domain. Voltammetric responses show transient diffusion-migration features at higher scan rates and quasi-steady state features at lower scan rates. Inherent microbead conductivity is shown to be linked to two resistive elements, electrolyte concentration dependent and independent, in series. The effects of phosphate binding are revealed as transient pattern in impedance spectroscopy data. Preliminary data suggest phosphate concentration-dependent peak features in the imaginary impedance versus frequency plot due to phosphate binding into the microbead.

Keywords Ion exchange · Pore resistivity · Ion selectivity · Desalination · Transport

Introduction

New high surface area materials play an important role in the development of desalination and electrosorption technologies, and over the recent years, metal–organic framework materials [1], doped graphene xerogels [2], graphene nanocomposites [3], microporous carbons [4], or carbon xerogels [5] have been employed, for example, in capacitive desalination. In contrast to these electrically conducting high surface area materials, traditional ion exchanger materials with high surface area and ion binding capacity have been developed based on polymer or polymer-inorganic hybrids [6]. The use of hydrous iron oxide as electrosorption material (particularly for arsenate and phosphate) in conjunction with high surface area carbons [7] and with ion exchanger membranes [8] has been explored.

Ion exchanger microbeads are widely applied in demineralisation and purification of water [9, 10], although not usually employed as membrane material. Theoretical models have been developed for transport phenomena in microbeads including surface and bulk diffusion [11]. Phosphate in particular, as a nutrient and as a waste stream component, has been targeted for removal based on microbeads in packed column systems [12]. Specific resins with appropriate ion selectivity and binding ability, for example, for phosphate and arsenate anions, are important in the treatment of waste but also in the purification and provision of potable water. Although usually employed in bulk in packed columns, it is interesting to explore the properties of resin microbeads individually in a membrane.

The FerrIX™ resin microbeads have a high content of iron oxides to enable specifically phosphate [13] and arsenate adsorption and removal [14].The behaviour and performance of FerrIX™ in fixed bed column reactors have been investigated and modelled quantitatively [15]. The microbeads are typically 0.3 to 0.5 mm in diameter and usually employed in large columns or flow reactors. Here, a single microbead is investigated at a time. The microbead

✉ Frank Marken
   f.marken@bath.ac.uk

[1] Department of Chemistry, University of Bath, Claverton Down, Bath BA2 7AY, UK

[2] Stichting Imec Nederland Within OnePlanet Research Center, Bronland 10, 6708 WH Wageningen, The Netherlands

[3] Materials & Chemical Characterisation Facility, University of Bath, MC2 BA2 7AY Bath, UK

is mounted into a thin epoxy film to leave the microbead exposed to electrolyte solution at both ends. Voltammetry and impedance measurements (in 4-electrode configuration) reveal ion mobility, exchange, and resin properties. The effects of phosphate anions on the electrochemical characteristics of a FerrIX™ microbead are investigated.

Figure 1A shows an illustration of an individual resin microbead with approximately spherical shape. After mounting into epoxy, a film is obtained with approximately 0.3- to 0.5-mm thickness and with a single microbead creating a central ion-conducting pathway (Fig. 1B, C). The film is mounted into a membrane voltammetry cell (Fig. 1D) with conventional four-electrode configuration: working and sense electrode in the r.h.s. compartment and counter and reference electrode in the l.h.s. compartment. Effects of electrolyte concentration and type are investigated

The aim of this study is to explore ion transport within the microbead and in the access regions of single immobilised microbeads fundamentally and at the scale of a single microbead, to investigate effects originating from the selectivity of the microbead to specific ions, to explore effects of phosphate binding, and to study new opportunities for single microbead micro-devices for water purification and ion sensing.

Experimental

Chemicals

Inorganic salts NaCl, LiCl, KCl, KNO_3, KOH, KH_2PO_4, $KClO_4$, and HCl (37 wt%, ACS reagent) were obtained from Sigma-Aldrich in analytical reagent purity and used without further purification. Demineralised water (resistivity 18.2 Ω cm at 20 °C) was taken from a Thermo Scientific water purification system.

Instrumentation

An Autolab PGSTAT12 potentiostat (Metrohm UK) was used for 4-electrode voltammetry in a custom-build cell [16]. Platinum wires served as working and counter electrode, and saturated Ag/AgCl reference electrodes (REF201, Hach Ltd.) were employed as reference and sense electrodes. A Modulab potentiostat (Solartron, UK) was employed for electrochemical impedance spectroscopy. All electrochemical experiments were performed in 4-electrode configuration (see Fig. 1D). Impedance data were at 0.0 V with an amplitude of 30 mV.

Characterisation of materials was performed with an Autosorb iQ (Quantachrome® ASiQwin™- Automated Gas Sorption) and with a scanning electron microscope (SEM) and energy-dispersive x-ray emission spectroscopy (EDX) on an Hitachi SU-3900 SEM with attached Oxford Instruments Ultim Max 170 mm^2 EDX detector system.

Procedures

FerrIX™ A33E microbeads (see optical micrograph in Fig. 2A) were obtained from Purolite Ltd. The material was characterised by scanning electron microscopy (SEM) and by nitrogen adsorption isotherm analysis (Brunauer–Emmett–Teller or BET; at 77 K; see Fig. 2B) which suggests mesopores predominantly in the range from 2 to 20 nm.

Mounting of individual microbeads in epoxy films was achieved with Teflon support films (FEP film for DLP 3D printer, Hawkung, China). A single microbead was placed onto a Teflon film and surrounded with freshly prepared epoxy resin (two component resin, PRESI Ltd., Resin MA2 +). A second Teflon film is then placed over the bead, and capillary forces allow the freshly mixed liquid epoxy resin to surround the microbead (avoiding inclusion of air bubbles). A 50-g weight applied to the top ensures that the
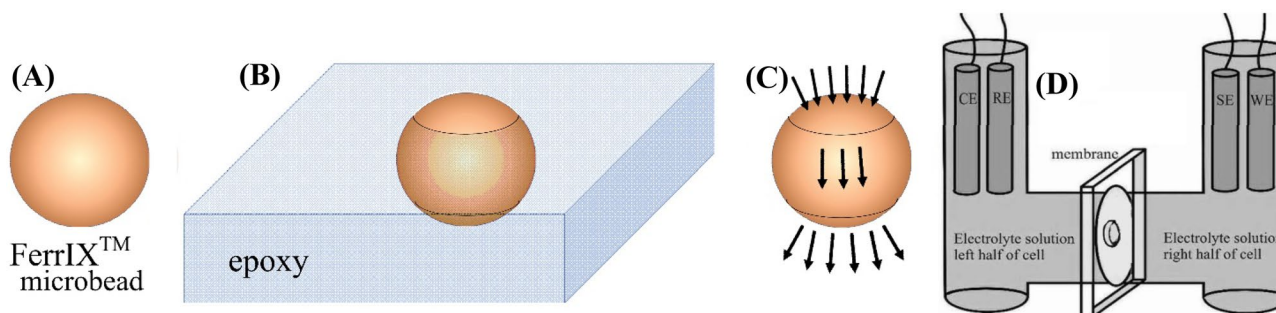

Fig. 1 Schematic of **A** a FerrIX™ microbead, **B** a microbead mounted into an epoxy film, **C** the anticipated ion transport path through the mounted bead, and **D** the four-electrode measurement cell with r.h.s. compartment (with working and sense electrode) and l.h.s. compartment (with counter and reference electrode)
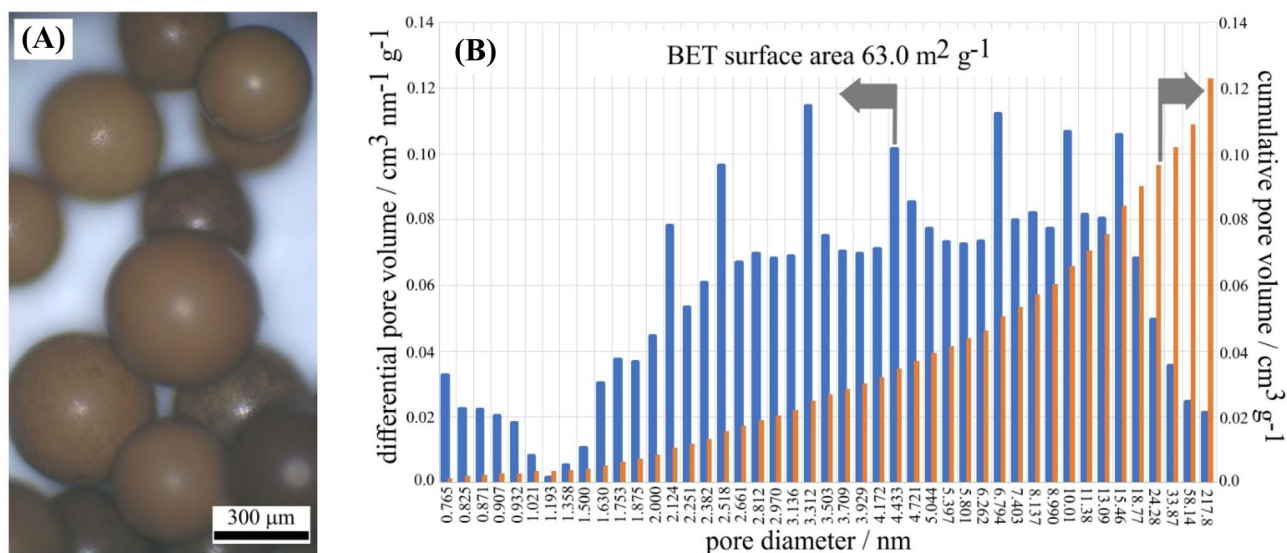
Fig. 2 A Optical micrograph of FerrIX™ particles. **B** Pore size distribution data from BET nitrogen binding isotherm data (BET surface area 63.0 m² g⁻¹) for FerrIX™ microbeads (pore size distribution analysis based on Barrett-Joyner-Halenda (BJH) calculation assuming cylindrical pores)

microbead is embedded at the thickest point of the epoxy film, which is allowed to set and harden (over 24 h at ambient conditions). Once removed from the Teflon films, the epoxy membrane is mounted in Kapton film (RS Components Ltd.) to fit into the electrochemical cell assembly.

Data from scanning electron microscopy (SEM) of unmounted and mounted microbeads are shown in Fig. 3. A spherical microbead with approximately 0.5-mm diameter can be seen to have a high elemental content of Fe, O, and S due to the presence of iron oxide and a sulphonate-based polymer backbone. The surface shows some porosity features with some bigger pores in the micron range. When mounted, the microbead is surrounded by a carbon-rich polymer. The presence of iron and sulphur elements is still clearly observed. The surface appears to be slightly modified in some regions, which is attributed here to a little bit of epoxy filling in bigger pores. Both SEM and optical micrographs (not shown) suggest that the microbead is on both sides open and accessible to electrolyte.

Results and discussion

Microbead electrochemistry in aqueous KCl

When placing aqueous KCl electrolyte into the two compartments of the membrane voltammetry cell (both sides with the same concentration), a concentration-dependent voltammetric response is obtained. A higher KCl concentration causes a higher ion current through the microbead (Fig. 4A). The slope of the current–potential curve at 0.0 V is indicative of approximately 20, 10, and 5 KΩ resistivity for concentrations of 0.01 M, 0.1 M, and 1.0 M KCl, respectively. Based on the geometry of the epoxy-mounted FerrIX™ microbead, it is possible to estimate the corresponding specific microbead conductivity (in first approximation, ignoring that there are effects from access diffusion, and simply assuming a FerrIX™ filled cylindrical hole with 375- μm diameter (see Fig. 3G) and 500- μm length, see Fig. 3) as $\kappa = \frac{1}{resistivity} \times \frac{length}{area} = 0.23, 0.45$, and $0.90 \ \Omega^{-1} \ m^{-1}$, respectively. These values seem to indicate a non-linear dependence of conductivity on electrolyte concentration (associated with pore size effects) approaching a limit of approximately 1.0 $\Omega^{-1} \ m^{-1}$ for higher concentration electrolyte (vide infra).

The shape of voltammetric responses is affected by both the scan rate and the KCl concentration. Figure 4B shows the effect of changing the scan rate from 1.5 to 0.1 Vs⁻¹ in 10 mM KCl. At a slower scan rate, near steady-state features are observed (a sigmoidal curve), whereas at higher scan rate, peak features and transient shapes are observed. This is consistent with the size of the microbead exposed to the solution phase resulting in planar diffusion-migration and a concentration polarisation effect. At a high KCl concentration (Fig. 4C), the distinction between transient and steady state features is lost and only ohmic behaviour dominates over the full potential range. This can be explained by transport within the microbead becoming rate limiting for higher KCl concentrations compared to the case of external transport and concentration polarisation causing rate limitations for lower KCl concentrations. The specific conductance for KCl electrolyte at 18 °C is κ = 1.11 $\Omega^{-1} \ m^{-1}$ for 0.1 M KCl and κ = 9.82
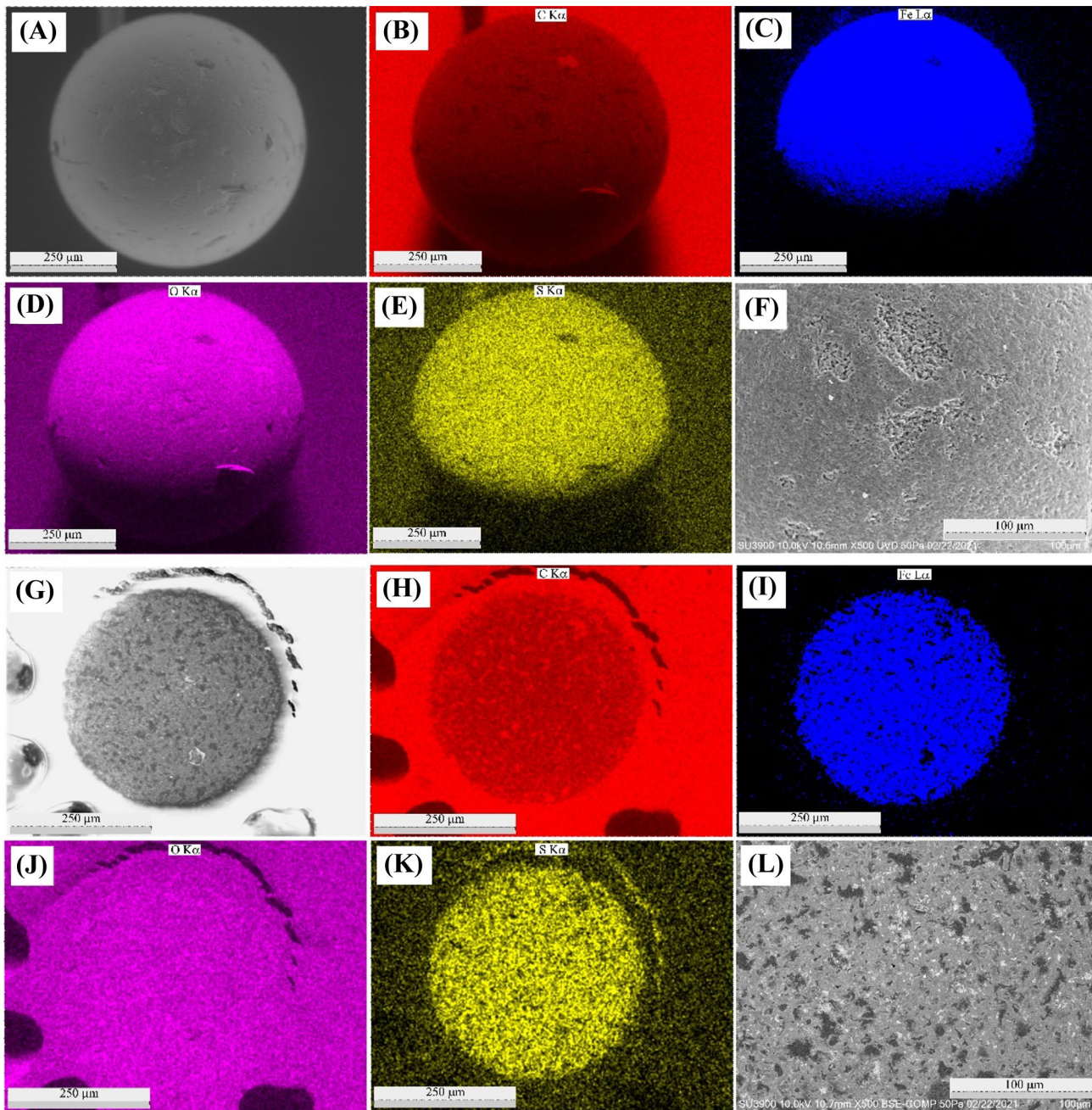
Fig. 3 **A–F** SEM and EDX data for a single micro-bead on a carbon surface. The main components in the micro-bead are C, Fe, O, and S. The surface can be seen to be porous with pores in the micro-meter range (**F**). **G–L** SEM and EDX data for a single micro-bead mounted in epoxy. The main components in the micro-bead are C, Fe, O, and S. The surface can be seen to be porous with some pores filled with epoxy (L)

Ω^{-1} m^{-1} for 1.0 M KCl [17]. Based on this comparison, it can be estimated that the specific conductivity of the microbead appears to limit within the range of 1 to 10 Ω^{-1} m^{-1}.

At the lower concentration of 10 mM KCl, three potential domains are apparent in data from cyclic voltammetry: (I) at low bias potential an ohmic region (0.0 to 0.5 V positive or negative), (II) at intermediate bias a plateau region probably associated with concentration polarisation (0.5 V to 2.0 V

positive or negative), and (III) at higher bias a further increase in current possibly linked to over-limiting conditions, e.g., involving convection (> 2.0 V positive or negative).

When employing asymmetric electrolyte concentration conditions (see Fig. 5), the voltammetric responses show a characteristic switch in behaviour between negative potential domain and positive potential domain. In the positive potential domain, the solution in the counter electrode compartment dominates.
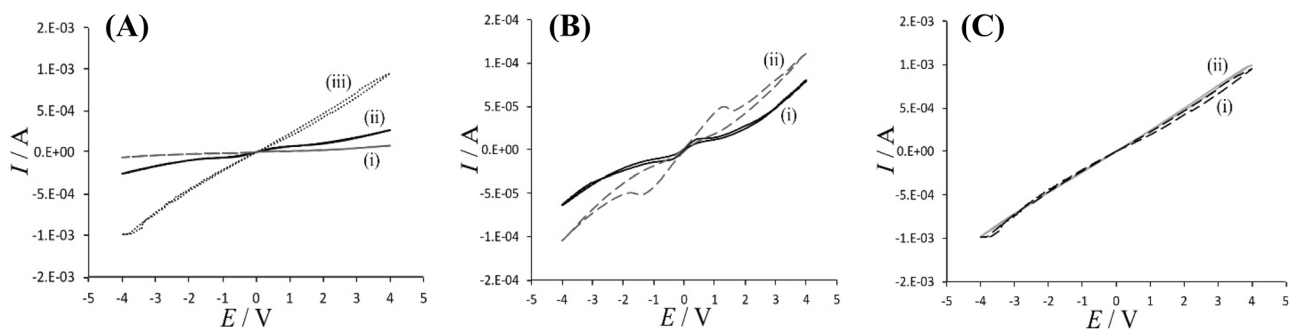
Fig. 4 **A** Cyclic voltammograms (scan rate 0.1 Vs^{-1}) for a FerrIX™ micro-bead in (i) 0.01 M, (ii) 0.1 M, and (iii) 1.0 M KCl on both sides. **B** Cyclic voltammograms (scan rate (i) 0.1 Vs^{-1} and (ii) 1.5 Vs^{-1}) in 0.01 M KCl. **C** As before, but in 1.0 M KCl

In the negative potential domain, the solution in the working electrode compartment dominates. This can be explained by semipermeability and anion transport through the microbead dominating over cation transport. If anions are driven by the potential from the high concentration reservoir through the bead, the current is high. When anions are driven from low to high-concentration side, the current is low. Figure 5D shows an illustration indicating the concentration-dependent anion movement as the key transport mechanism. The high concentration side (see negative potential domain) shows less good match of currents, which could be associated with some

additional membrane polarisation close to the low concentration solution compartment. Hydrous ferric oxide materials are known to exhibit a predominantly positive surface potential with p.z.c. at approximately pH 8 [18], which could explain the exclusion of cations and the predominant transport of anions.

Next, impedance spectroscopy data for the microbead in a symmetric measurement cell are shown (Fig. 6). At higher frequencies, a semi-circular feature is observed consistent with a parallel resistor (Rp) and capacitor (C) in addition to a series resistor (Rs). The capacitor consistently shows a value of approximately 30 pF (independent of KCl concentration),
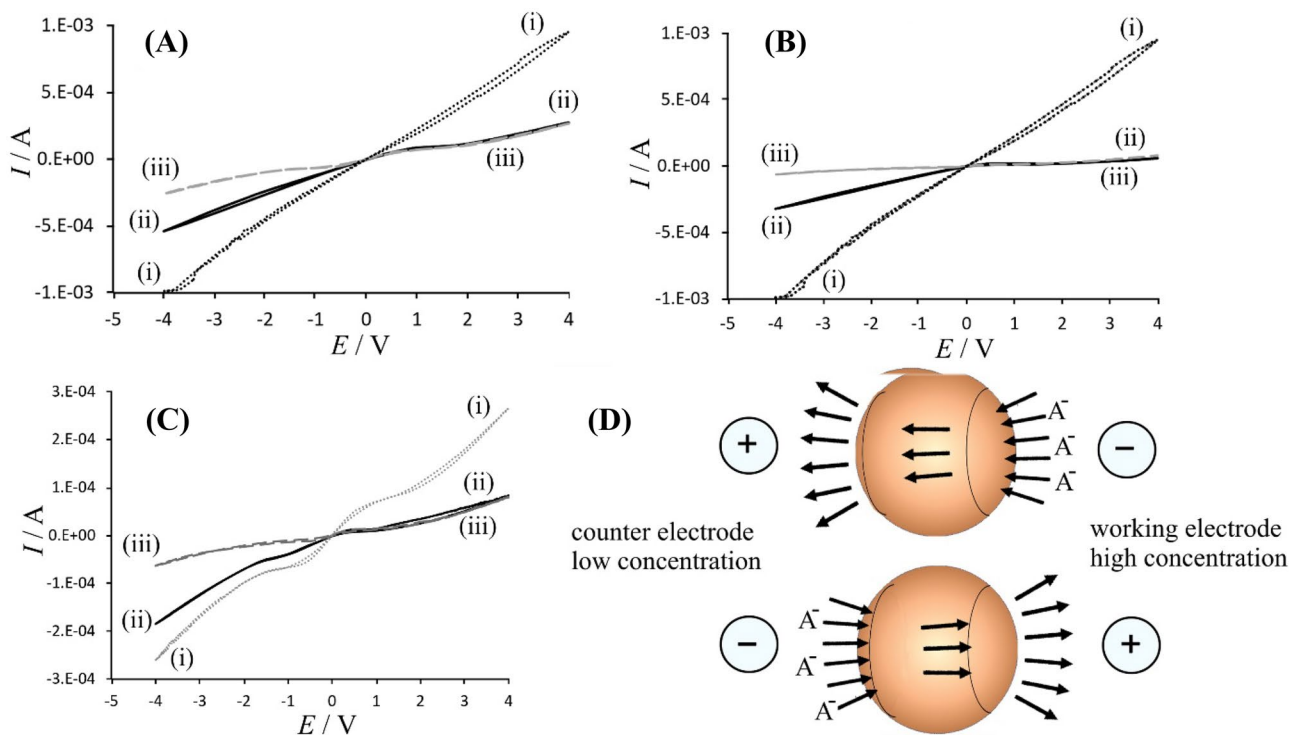

Fig. 5 **A** Cyclic voltammograms (scan rate 0.1 Vs^{-1}) for a FerrIX™ microbead with l.h.s./r.h.s. (i) 1.0/1.0 M KCl, (ii) 0.1/1.0 M KCl, and (iii) 0.1/0.1 M KCl. **B** As before, but with l.h.s./r.h.s. (i) 1.0/1.0 M KCl, (ii) 0.01/1.0 M KCl, and (iii) 0.01/0.01 M KCl. **C** As before,

but with l.h.s./r.h.s. (i) 0.1/0.1 M KCl, (ii) 0.01/0.1 M KCl, and (iii) 0.01/0.01 M KCl. **D** Illustration of concentration effects on anion transport through microbeads for the case of l.h.s./r.h.s. low/high concentration
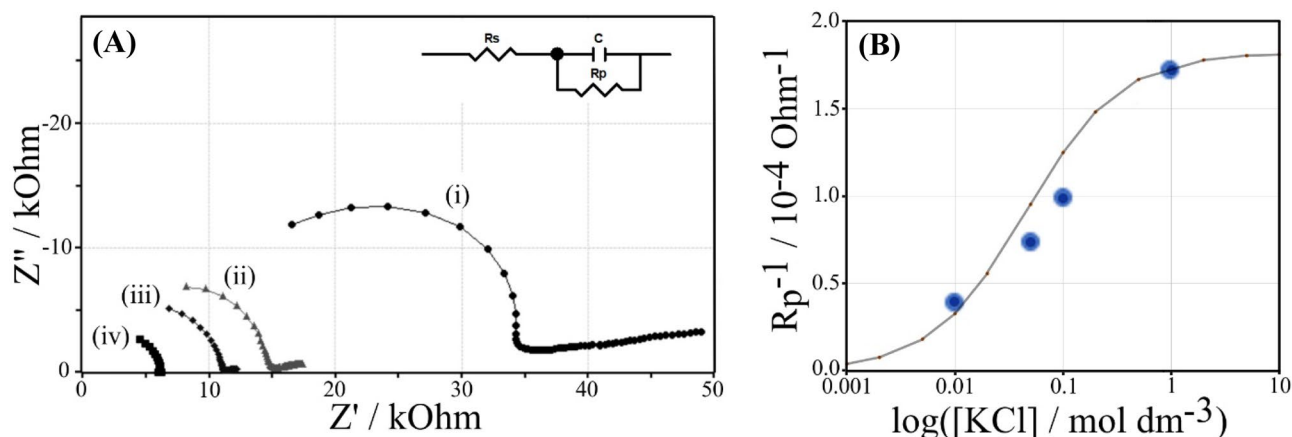
Fig. 6 A Impedance spectroscopy data (4-electrode configuration; at 0.0 V; frequency range 300 kHz to 0.1 Hz; amplitude 30 mV) for a FerrIX™ microbead with l.h.s./r.h.s. (i) 0.01/0.01 M KCl, (ii) 0.05/0.05 M KCl, (iii) 0.1/0.1 M KCl, and (iv) 1.0/1.0 M KCl. **B** Plot of Rp^{-1} versus logarithm of KCl concentration. The line indicates a model for two resistors in series: one with 5500 Ohm and one with a concentration dependent resistance of (250/[KCl]) Ohm

which is assigned here to the charging of the epoxy film holding the FerrIX™ microbead. The resistor Rp represents the high-frequency resistivity of the microporous FerrIX™ microbead (with contributions from the electrolyte close to the microbead [8]). Perhaps interestingly, the value for Rp is (in part) KCl concentration dependent. There appear to be two components based on (i) a resistor that is inversely proportional to the KCl concentration as would be expected for access diffusion [8] and electrolyte filled pore regions and (ii) a resistor that remains constant associated with smaller pores. Figure 6B shows a plot of Rp^{-1} data and a fitted simplistic model (the two resistors in series, one electrolyte concentration dependent and one independent) with fixed 5500 Ohm and a concentration dependent resistance of (250/[KCl]) Ω. For high concentrations of KCl, the value of Rp is dominated solely by the fixed resistance of 5500 Ω. This could be assigned to resistance of smaller micropore spaces that are not fully electrolyte-filled due to exclusion of cations [19]. Perhaps interestingly, the value of 5500 Ω (equivalent to $\kappa = 0.8$ Ω^{-1} m^{-1}) is approximately consistent with the transition point for concentration polarisation to be observed (at lower concentration) and not observed (at higher concentration) (vide supra).

An additional feature in the impedance data is a lower frequency "tail" with only very little imaginary impedance contribution. This is observed clearly at lower KCl concentration, but not at 1.0 M KCl. This feature is therefore linked to concentration polarisation and consistent with observations in the data from voltammetry experiments (vide supra). For the small microbead (and at the given time scale), predominantly real impedance is detected (drifting to higher impedance at lower frequencies) probably associated with dominating spherical diffusion-migration of electrolyte in the solution phase adjacent to the microbead.

Microbead electrochemistry in aqueous electrolyte: cation and anion effects

Effects of electrolyte cations and anions were investigated in symmetric solution cells with 0.1 M electrolyte. Figure 7 shows data for H^+, Li^+, Na^+, and K^+ in the form of chloride salts. Currents show characteristic trends which seem linked at least in part to cation diffusivity. The experiment in 0.1 M HCl appears to result in the highest currents. However, these effects could be linked to the effect of the cation on concentration polarisation rather than indicating cation transport through the membrane. The effect of scan rate suggests a similar transition from steady state to transient when going from lower to higher scan rates in all cases.

Data in Fig. 8 show the effect of the electrolyte anion (for 0.1 M K^+ salts) on the voltammetric responses. A similar sequence is observed with larger anions such as phosphate and perchlorate lowering the current. Changes in the ohmic region in potential domain I could be due to the micro-bead changing conductivity due to better anion binding. After performing experiments with phosphate and with perchlorate, the membrane needed to be re-equilibrated in distilled water for 24 h to re-cover the properties in aqueous KCl. This suggests that binding of phosphate but also interaction with hydrophobic and larger anions like perchlorate occurs with more time required for re-equilibration (release of bound anions).

Microbead impedance measurements in aqueous electrolyte: effects of phosphate

The interaction with binding anions (such as phosphate) is likely to modify the characteristics of the microbead. FerrIX™ materials are known to strongly interact with
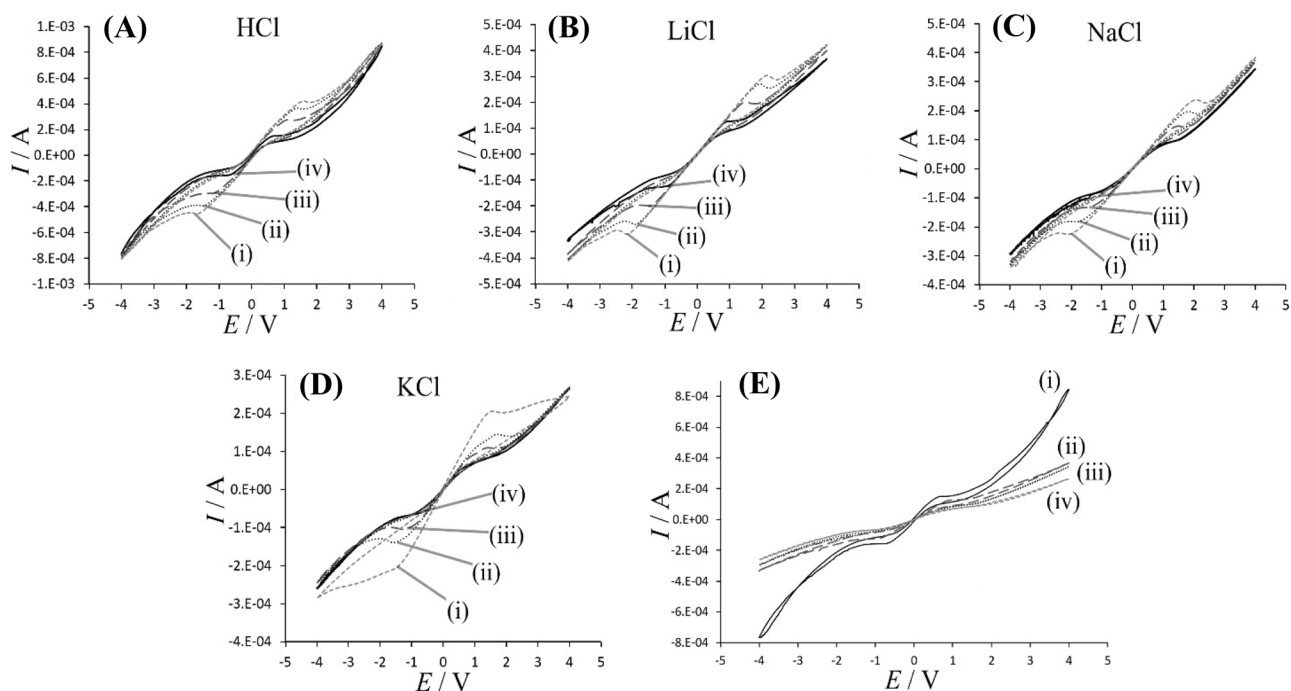
Fig. 7 Cyclic voltammograms (scan rate (i) 1.5, (ii) 1.0, (iii) 0.5, and (iv) 0.1 Vs^{-1}) for a FerrIX™ microbead with l.h.s./r.h.s. **A** 0.1/0.1 M HCl, **B** 0.1/0.1 LiCl, **C** 0.1/0.1 M NaCl, and **D** 0.1/0.1 M KCl. **E** Cyclic voltammograms (scan rate 0.1 Vs^{-1}) for a FerrIX™ microbead with l.h.s./r.h.s. (i) 0.1/0.1 M HCl, (ii) 0.1/0.1 LiCl, (iii) 0.1/0.1 M NaCl, and (iv) 0.1/0.1 M KCl

phosphate (or also arsenate) anions. Therefore, additional electrochemical impedance spectroscopy experiments are performed in phosphate electrolyte. From cyclic voltammetry data in Fig. 8D, there appeared to be no significant change in the presence of phosphate apart from a lowering of currents. Figure 9A shows a set of impedance spectra obtained with symmetric 10 mM phosphate buffer pH 7 on both sides of the microbead approximately 2, 4, 6, and 8 min
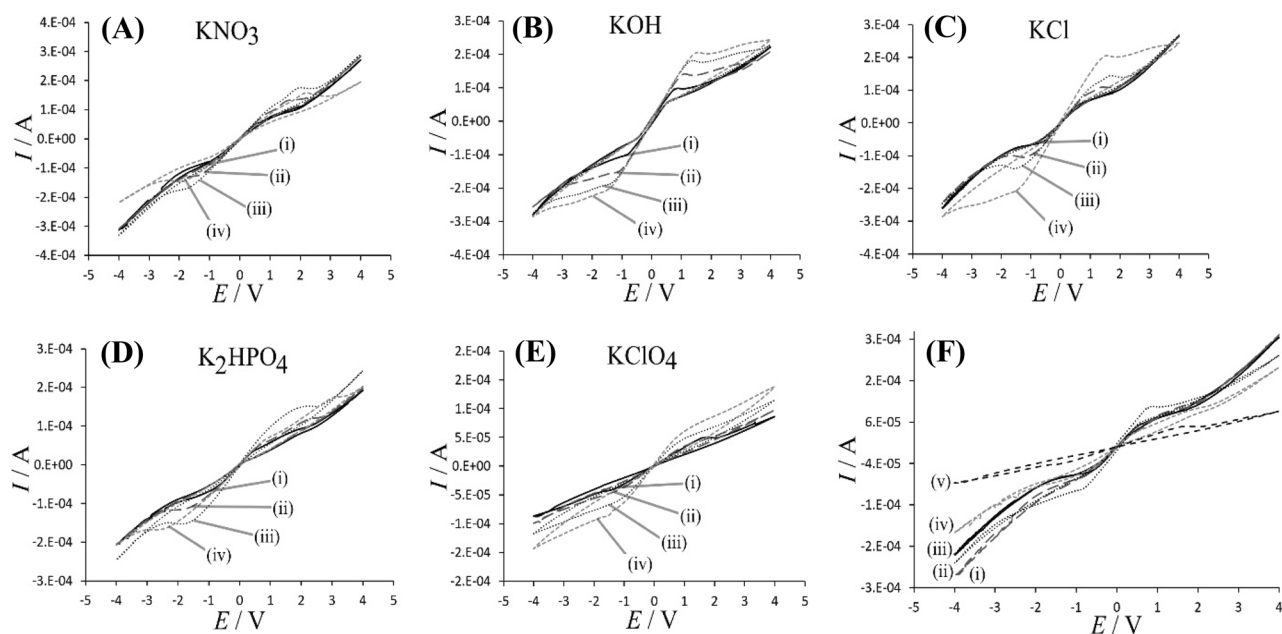

Fig. 8 Cyclic voltammograms (scan rate (i) 0.1, (ii) 0.5, (iii) 1.0, and (iv) 1.5 Vs^{-1}) for a FerrIX™ bead with l.h.s./r.h.s. electrolyte solution in **A** in 0.1 M KNO$_3$, **B** KOH, **C** KCl, **D** K$_2$HPO$_4$, and **E** KClO$_4$. **F** Cyclic voltammograms (scan rate 0.1 Vs^{-1}) for a FerrIX™ bead with l.h.s./r.h.s. 0.1 M electrolyte solution comparing (i) KNO$_3$, (ii) KOH, (iii) KCl, (iv) K$_2$HPO$_4$, and (v) KClO$_4$
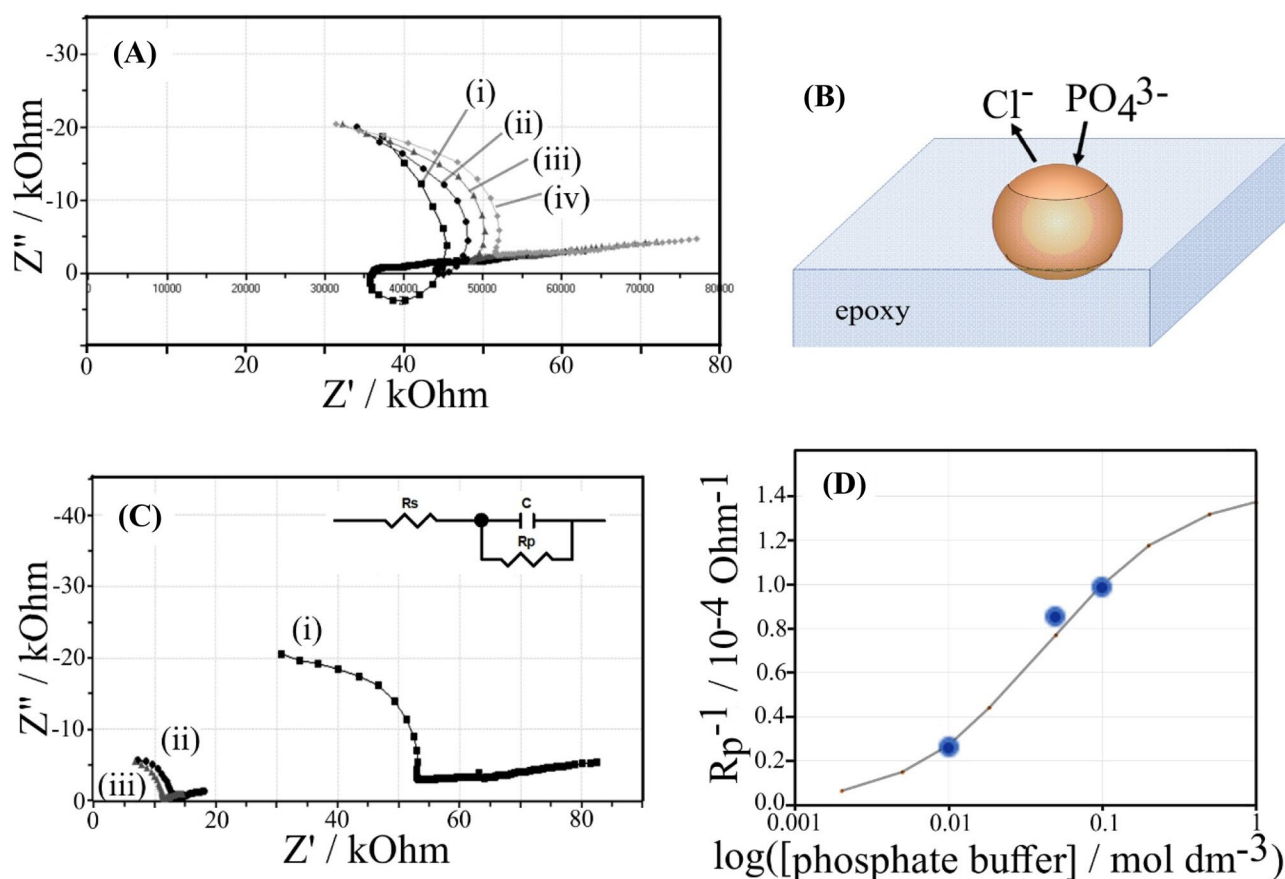
Fig. 9 **A** Impedance spectroscopy data (4-electrode configuration; at 0.0 V; frequency range 300 kHz to 0.1 Hz; amplitude 30 mV) for a FerrIX™ microbead with l.h.s./r.h.s. 0.01/0.01 M phosphate buffer pH 7. **B** Illustration of the chloride versus phosphate exchange. **C** Impedance spectroscopy data (at 0.0 V; frequency range 300 kHz to 0.1 Hz; amplitude 30 mV) for a FerrIX™ microbead equilibrated with l.h.s./r.h.s. (i) 0.01/0.01 M phosphate buffer, (ii) 0.05/0.05 M phosphate buffer, and (iii) 0.1/0.1 M phosphate buffer pH 7. (**D**) Plot of Rp^{-1} versus logarithm of phosphate buffer concentration. The line indicates an approximate model for two resistors in series: one with 7000 Ohm and one with a concentration dependent resistance of $(300/[KCl])$ Ohm

after filling the electrochemical cell. Spectra are clearly time-dependent, and especially early on during the experiment, complex inductive behaviour (loops) is detected, possibly associated with phosphate binding (non-equilibrium). With time, these loops disappear (presumably due to phosphate binding going to completion). However, the time dependence appears to be a significant feature especially for lower concentration of phosphate without sufficient time for phosphate binding to go to equilibrium.

The resistance Rp was determined for 10 mM, 50 mM, and 100 mM phosphate buffer pH 7 (Fig. 9D) in order to compare the behaviour to that observed for KCl (see Fig. 6). Very similar behaviour is observed, and a plot of Rp^{-1} versus logarithm of phosphate buffer concentration reveals a similar trend. There are two resistive components in series with one electrolyte concentration–independent resistance dominating at high concentrations and essentially limiting the value for Rp. This concentration-independent resistance may again be associated with smaller micropores.

Further experiments were conducted a lower phosphate concentration and for phosphate only present in the r.h.s. compartment of the electrochemical cell. Figure 10 shows data obtained with impedance spectroscopy over the frequency range 300 kHz to 100 Hz. Data in the Nyquist plot suggest that addition of phosphate causes gradual changes. Plots of Z'' show the effects of phosphate addition most clearly. In Fig. 10A, a slight indication of a peak feature appears in the presence of 0.1 mM phosphate (see curve ii). When adding more phosphate, this peak feature becomes very clear. At the position of the peak, the value for Z'' (phosphate) can be obtained and divided by the Z'' in the absence of phosphate. A plot is shown in Fig. 10D (iv) with a monotonic trend for increasing phosphate concentration. Z'' is associated with capacitance changes probably due to binding of phosphate and therefore potentially selective for phosphate. More detailed experiments will be necessary to explore the exploitation of this change in Z'' for phosphate sensing.
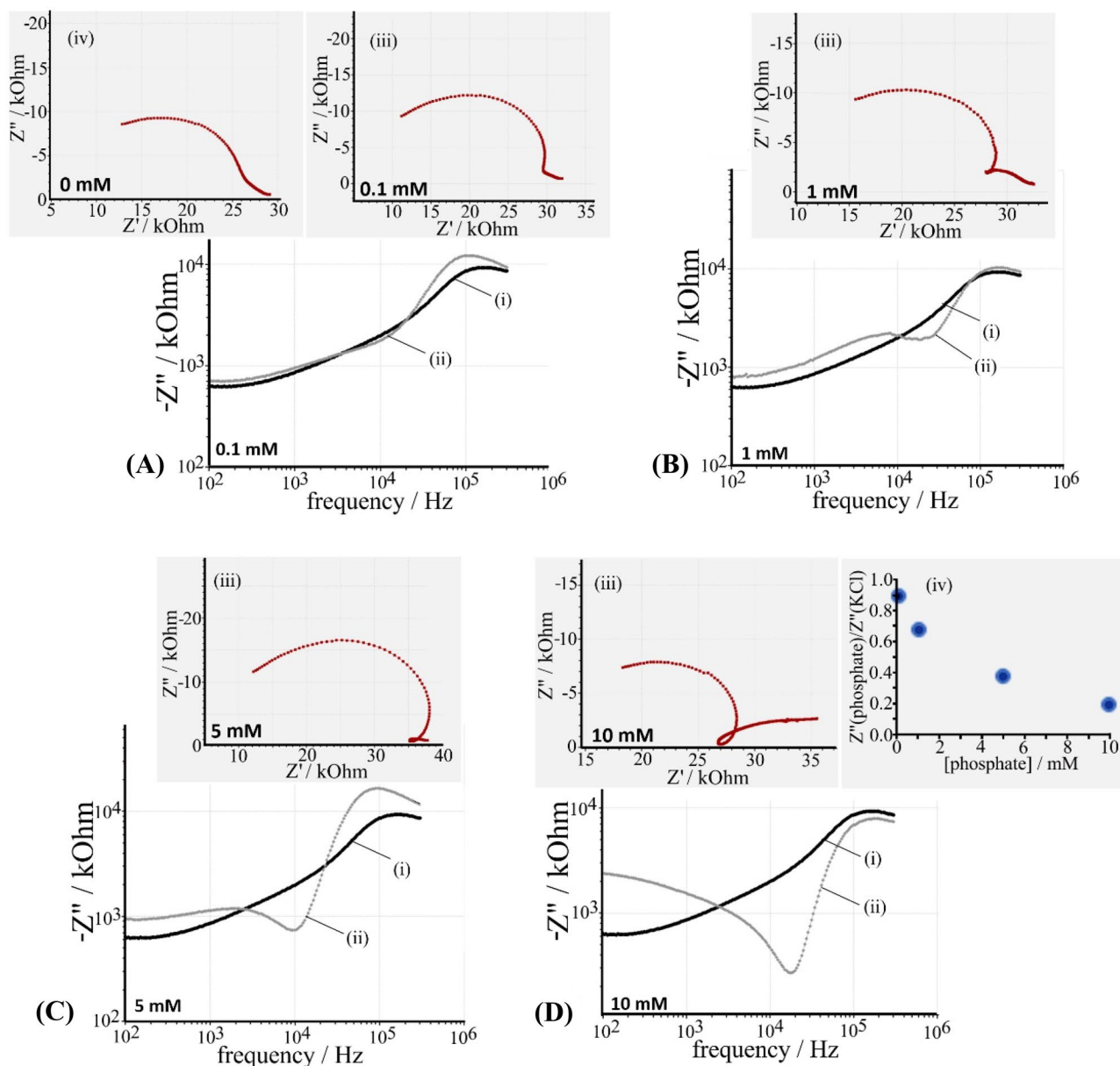
Fig. 10 Impedance spectroscopy data (0.0 V vs. OCP, 300 kHz to 100 Hz, 20-min equilibration after adding phosphate) for 10 mM KCl on both sides and addition of phosphate buffer pH 7 on the r.h.s. (working electrode): **A** (i) plot of Z″ versus frequency for 10 mM KCl only and (ii) with 0.1 mM phosphate buffer added, (iii) Nyquist plot, and (iv) Nyquist plot for 10 mM KCl only. **B** (i) plot of Z″ versus frequency for 10 mM KCl only and (ii) with 1.0 mM phosphate buffer added, (iii) Nyquist plot. **C** (i) plot of Z″ versus frequency for 10 mM KCl only and (ii) with 5.0 mM phosphate buffer added, and (iii) Nyquist plot. **D** (i) plot of Z″ versus frequency for 10 mM KCl only and (ii) with 10 mM phosphate buffer added, (iii) Nyquist plot, and (iv) plot of Z″ (phosphate)/Z″ (KCl) versus phosphate buffer concentration

Summary and conclusions

A single FerrIX™ microbead embedded into a thin film of epoxy has been investigated as a membrane in a 4-electrode electrochemical cell. Both exploratory voltammetry and impedance data suggest that microbead conductivity changes depend on electrolyte concentration. Experiments with different electrolyte concentrations in l.h.s. and r.h.s. compartments reveal that anion transport dominates. The main observations are as follows:

- The microbeads allow transport of anions (semipermeability due to small pores causing exclusion of cations [20]) under conditions of applied potential. Voltammetry experiments with varying levels of electrolyte and with various types of electrolyte suggest a dominant role of anion transport.

- In voltammetry experiments and at concentrations of electrolyte lower than approximately 1 M, there are three potential domains based on (i) ohmic behaviour, (ii) concentration polarisation behaviour, and (iii) over-limiting behaviour. These phenomena are linked to microbead specific conductivity being higher compared to bulk electrolyte specific conductivity.
- In electrochemical impedance spectroscopy experiments, a transition from high-frequency behaviour (with semi-circle in the Nyquist plot) to low-frequency behaviour (ohmic for high electrolyte concentration and drifting ohmic at lower electrolyte concentration) is observed consistent with data from voltammetry.
- The resistance of the microbead extracted from fitting the high-frequency semicircle data shows an inverse dependency on electrolyte concentration at low concentration and a limit in conductivity (Rp becomes essentially constant) at higher electrolyte concentration consistent with very small pores dominating/limiting conductivity at high electrolyte concentration.
- For binding anions such as phosphate, a drift in the impedance data (and an inductive loop) signifies effects from anion absorption into the FerrIX™ microbead. For lower phosphate concentration, this leads to a characteristic peak in imaginary impedance versus frequency data as a function of phosphate concentration.

Overall, the electrochemical experiments with the epoxy-mounted microbeads provide new insights into the processes inside/outside the microbead and into the interaction with electrolyte media. More work will be necessary to further explore ion transport and chemical mechanisms in microbeads, for example, in conjunction with water splitting [21]. Individual microbeads in membranes can respond to binding anions, and this may lead to new microdevices which could be exploited in future, for example, for sensing or monitoring phosphate or arsenate.

References

1. Cen BQ, Li KX, Lv CC, Yang R (2020) A novel asymmetric activated carbon electrode doped with metal-organic frameworks for high desalination performance. J Solid State Electrochem 24:687–697
2. Wang SS, Feng JW, Meng QH, Cao B, Tian GY (2019) Study on boron and nitrogen codoped graphene xerogel for high-performance electrosorption application. J Solid State Electrochem 23:2377–2390
3. Wei YC, Huo YQ, Tian GY, Meng QH, Cao B (2016) Nitrogen-doped functional graphene nanocomposites for capacitive deionization of NaCl aqueous solutions. J Solid State Electrochem 20:2351–2362
4. Biesheuvel PM, Porada S, Levi M, Bazant MZ (2014) Attractive forces in microporous carbon electrodes for capacitive deionization. J Solid State Electrochem 18:1365–1376
5. Zafra MC, Lavela P, Rasines G, Macias C, Tirado JL (2014) Effect of the resorcinol/catalyst ratio in the capacitive performance of carbon xerogels with potential use in sodium chloride removal from saline water. J Solid State Electrochem 18:2847–2856
6. Alabi A, AlHajaj A, Cseri L, Szekely G, Budd P, Zou LD (2018) Review of nanomaterials-assisted ion exchange membranes for electromembrane desalination. NPJ Clean Water 1:10
7. Dai M, Zhang M, Xia L, Li YM, Liu YY, Song SX (2017) Combined electrosorption and chemisorption of As(V) in water by using FerGO@AC electrode. ACS Sustain Chem Engineer 5:6532–6538
8. Sivasothy T, Ndifor-Angwafor NG, Marken F (2018) Voltammetric characteristics of hydrous Fe(III) oxide embedded into Nafion and immobilised onto a screen-printed carbon electrode: binding of arsenate versus phosphate. J Solid State Electrochem 22:3059–3067
9. Martin BD, Parsons SA, Jefferson B (2009) Removal and recovery of phosphate from municipal wastewaters using a polymeric anion exchanger bound with hydrated ferric oxide nanoparticles. Water Sci Technol 60:2637–2645
10. Das Gupta M, Loganathan P, Vigneswaran S (2012) Adsorptive removal of nitrate and phosphate from water by a purolite ion exchange resin and hydrous ferric oxide columns in series. Sep Sci Technol 47:1785–1792
11. Koh JH, Wankat PC, Wang NHL (1998) Pore and surface diffusion and bulk-phase mass transfer in packed and fluidized beds. Ind Engineer Chem Res 37:228–239
12. Cordell D, Drangert JO, White S (2009) The story of phosphorus: Global food security and food for thought. Global Environm Change Human Policy Dimensions 19:292–305
13. Nur T, Johir MAH, Loganathan P, Nguyen T, Vigneswaran S, Kandasamy J (2014) Phosphate removal from water using an iron oxide impregnated strong base anion exchange resin. J Ind Engineer Chem 20:1301–1307
14. Chiavola A, D'Amato E, Gavasci R, Sirini P (2015) Arsenic removal from groundwater by ion exchange and adsorption processes: comparison of two different materials. Water Sci Technol Water Supply 15:981–998
15. Nur T, Shim WG, Johir MAH, Vigneswaran S, Kandasamy J (2014) Modelling of phosphorus removal by ion-exchange resin (Purolite FerrIX A33E) in fixed- bed column experiments. Desal Water Treatment 52:784–790
16. Brown R, Madrid E, Castaing R, Stone JM, Squires AM, Edler KJ, Takashina K, Marken F (2017) Free-standing phytantriol Q(224)

cubic-phase films: Resistivity monitoring and switching. ChemE-lectroChem 4:1172–1180

17. Harned HS, Owen BB, (1958) The Physical Chemistry of Electrolyte Solutions. Reinhold Publishing Corp., New York, p. 197

18. Pretorius PJ, Linder PW (1998) Determination of Diffuse Double Layer protonation constants for hydrous ferric oxide (HFO): supporting evidence for the Dzombak and Morel compilation. Chem Spec Bioavailability 10:115–119

19. Wang RY, Lin SH (2021) Pore model for nanofiltration: History, theoretical framework, key predictions, limitations, and prospects. J Membrane Sci 620:118809

20. Schmid G (1998) Electrochemistry of capillary systems with narrow pores. 1. Overview J Membrane Sci 150:151–157

21. Kang MS, Choi YJ, Lee HJ, Moon SH (2004) Effects of inorganic substances on water splitting in ion-exchange membranes I. Electrochemical characteristics of ion-exchange membranes coated with iron hydroxide/oxide and silica sol. J Coll Interface Sci 273:523–532